Peer-reviewed version available at Appl. Sci. 2018, 8, 1705; doi:10.3390/app8091705

Article

Effect of Cavity Vacuum Pressure Diminution on Thermal Performance of Triple Vacuum Glazing

Saim Memon [1]*, Farukh Farukh [2] and Karthikeyan Kandan [2]

[1] Centre for Advanced Materials, School of Engineering, London South Bank University, 103 Borough Road, London, SE1 0AA, UK
[2] Centre for Engineering Science and Advanced Systems, School of Engineering and Sustainable Development, De Montfort University, The Gateway, Leicester, LU1 9BH, UK; F.Farukh@dmu.ac.uk; karthikeyan.kandan@dmu.ac.uk
* Correspondence: S.Memon@lsbu.ac.uk; Tel.: +44-207-815-7510

Abstract: Long-term durability of the vacuum edge-seal plays a significant part in retrofitting triple vacuum glazing (TVG) to existing buildings in achieving towards zero-energy buildings (ZEB) target. Vacuum pressure decrement with respect to time between panes affect the thermal efficiency of TVG. This study reports a 3D finite element model, with validated mathematical methods and comparison, for the assessment of the influence of vacuum pressure diminution on the thermal transmittance (U value) of TVG. The centre-of-pane and total U values of TVG calculated to be 0.28 $Wm^{-2}K^{-1}$ and 0.94 $Wm^{-2}K^{-1}$ at the cavity vacuum pressure of 0.001 Pa. The results suggests that a rise in cavity pressure from 0.001 Pa to 100 kPa increases the centre-of-pane and total U values from 0.28 $Wm^{-2}K^{-1}$ and 0.94 $Wm^{-2}K^{-1}$ to 2.4 $Wm^{-2}K^{-1}$ and 2.58 $Wm^{-2}K^{-1}$, respectively. The temperature descent on the surfaces of TVG between hot and cold sides' increases by decreasing the cavity vacuum pressure from 50 kPa to 0.001 Pa. To maintain the cavity vacuum pressure of 0.001 Pa for over 20 years of life span in the cavity of 10 mm wide edge sealed triple vacuum glazing, non-evaporable getters will maintain the cavity vacuum pressure that will enable the long-term durability to TVG.

Keywords: vacuum pressure; triple vacuum glazing; finite element modelling; thermal performance; towards zero-energy buildings

1. Introduction

Carbon reduction is a global challenge due to an increase of average global annual temperature to 0.99°C with CO_2 level reached 400 ppm breaking the 1950's level threshold of 300 ppm [1]. Vacuum insulation as a retrofit solution to existing buildings play a momentous role in carbon reduction and towards zero-energy building (ZEB) target [2] as buildings are accountable for at least 30% of the overall global final energy consumed [3,4]. Although, a number of retrofitting measures to improve building insulation have made building sector already energy-efficient [5], but it requires advanced technologies that bring the building sector towards ZEB. A triple vacuum glazing (TVG) has a prospective to curtail heat flow between warm side and cold side, i.e. to provide preeminent thermal insulation so called thermal transmittance (U-value) [6]. Thermal transmittance of TVG primarily depends on the thickness of the glass panes, vacuum pressure in the space between the glass panes, emissivity of the coatings on glass pane, frame, type of spacers that separate the panes of glass and type of window frame. The total U-value consists of the influence of the frame and the area of edge-seal. The edge seal area is dependent on the width and the type of edge sealing material. Airtight edge seal of a TVG must be able to perpetuate vacuum pressure below 0.1 Pa for quelling gaseous heat-conduction for long-term duration [7]. Benson et al [8] investigated laser technology in a vacuum chamber to seal the edges of two glass panes. This achieved airtight edge seal but the cavity vacuum pressure was not below 0.1 Pa because laser seal instigated particles such as moisture and notorious

gases [9]. First successful fabrication method of double vacuum glazing relied on lead based solder glass material sealed at around 450°C (it was recognised as high-temperature sealing method) [10–11]. This method achieved centre-of-pane U value of 0.8 $Wm^{-2}K^{-1}$ and elevated at the commercial scale with a trade name of SPACIA. The problems with high-temperature method of sealing is degradation of soft (low emissivity) coatings only hard coatings can be used [12], if using annealed glass then loss of toughness, and require more amount of heat energy for the construction. Investigations on low-temperature solder glass material showed a hermetic edge seal, but durability was a problem due to the absorption of moisture [9]. Second successful fabrication method of double vacuum glazing used Indium or Indium-alloy; it sealed at low-temperature process about 160°C. It required secondary adhesive seal to prevent access from moisture [13]. A low-temperature sealing process enabled the use of low emittance soft coatings, reduces radiative heat-transfer between glass panes, and annealed glass allows to increase support pillar spacing, reduces conductive heat-transfer [14]. The problem with the low-temperature fabrication method is the use of semi-precious indium-alloy. It is a hindrance in advancing indium –sealed vacuum glazing at commercial level [15]. Recently, a new low-temperature composite materials and methods of fabrication reported in Memon et al. [16]. In which CS-186 type of Cerasolzer and steel reinforced epoxy by J-B resin [17] used for the development of composite edge sealed triple vacuum glazing.

Despite of aforementioned successful constructions of double and triple vacuum glazing, there is always an uncertainty of the degradation/leakage of the cavity vacuum pressure. It is also pertinent that during evacuation process or after sealing the pump-out tube of the TVG, there is a propensity of some gas molecules remained in the cavity that react when exposed to sunlight and/or under extreme climate conditions for longer time due to the production of carbon monoxide inside the cavity that degrades the vacuum layer. It is obvious that TVG exposed to sunlight and need to design to sustain at different climate temperatures in order to avoid degradation of vacuum. The heat conductance and internal pressure due to ageing (for over 250 days), with a temperature increased from ambient (21°C) to 150°C of a vacuum glazing was reported in Turner and Collins (1997) [18]. It showed that both pressure inside the cavity and heat conductance rose upon heating. It identified that the increase in the thermal conductance from the glass bulk due to the water vapour evolved into the gap was negligible; it was less than 0.1$Wm^{-2}K^{-1}$ over a period of 25 years at 30°C for the samples baked out at about 180°C for 1 hour. The result from mass-spectroscopy showed that 95% of the total remaining gas on the internal glass surfaces is water vapour whereas remaining 5% includes H_2, H_2O, CO/N_2, O_2 and CO_2. Fang et al (2009) [19] investigated the extreme temperature cycling effect for which the heat conductance at the centre-of-pane found to be increased about 10.2% (1.18 $Wm^{-2}K^{-1}$ to 1.30 $Wm^{-2}K^{-1}$) when the cavity vacuum-pressure inside the vacuum glazing had increased from 0.1 Pa to 0.16 Pa. According to N. Ng et al (2005) [20], investigation of evolved gases into the evacuated gap in vacuum glazing for which the samples of vacuum glazing were aged by exposing them to high temperatures and sunlight for a long period of time and their internal pressure and the existing gases were studied using a vacuum gauge and a mass-spectrometer, respectively. Yet, there is no literature available on the cavity vacuum pressure diminution influence on triple vacuum glazing (TVG). Thus, this paper reports the effects of vacuum pressure on thermal transmittance of TVG by developing mathematical model using finite element method in predicting their thermal performance.

This paper contributes to the new understanding of the effects of cavity vacuum pressure diminution on thermal performance (heat-transfer characteristics) of triple vacuum glazing. In this paper, a finite element method with details of governing equations utilised and modelled heat-transfer mechanisms of the 10 mm wide edge sealed triple vacuum glazing reported. The influence of vacuum pressure diminution on the thermal transmittance (U value) of a triple vacuum glazing when the vacuum space (cavity) pressure decreases from 0.001 Pa (high-vacuum pressure) to 101.321 kPa (atmospheric pressure).

Preprints (www.preprints.org) | NOT PEER-REVIEWED | Posted: 23 August 2018 doi:10.20944/preprints201808.0408.v1

Peer-reviewed version available at Appl. Sci. 2018, 8, 1705; doi:10.3390/app8091705

2. Materials and Methods

To analyse TVG thermal performance, a finite-element model using a validated approach developed based on the boundary conditions developed. It was quantified with a boundary conditions as: Temperature, $T = T(x,t)$; heat-flux(surface) per unit area, $q = q(x,t)$; heat flux (volumetric) per volume, $q = r(x,t)$; heat-transfer convection (surface), $q = h(T - T^o)$, (where film-coefficient $h = h(x,t)$ and temperature (sink) $T^o = T^o(x,t)$; and heat-transfer radiation $q = \mathfrak{C}[(T - T^z)^4 - (T^o - T^z)^4]$, where $\mathfrak{C}$ the radiation constant and T^z value of absolute zero on the temperature scale used. The heat conduction occurred as a solid body in which the conductivity subjected to the temperature, internal energy with effects of latent heat and convection and radiation equations. According to Green and Naghdi (1965) [21] the energy balance approach used is stated in eq. (1) and with the Fourier Law eq. (2) is acquired by applying the standard Galerkin spatial discretisation method.

$$\int_V \rho \dot{E} dV = \int_A q dA + \int_V r \, dV \quad (1)$$

$$\int_V \rho \dot{E} \delta T dV + \int_V \frac{\partial \delta T}{\partial x} . k . \frac{\partial T}{\partial x} dV = \int_V \delta T r dV + \int_{Aq} \delta T q dA \quad (2)$$

Where V is the volume of the glazing components having A area of the surface, r the heat supplied externally per volume, ρ the density of the materials, $\dot{E}$ the material time rate of the internal energy, q the heat flux/area. It is an adopted assumption that iterative solutions disjoined in a way that only $\dot{E} = \dot{E}(T)$, where T is the temperature of the material. δT Arbitrary differential field satiating the essential boundary conditions. The body estimated geometrically with finite elements, so the temperature interpolated as in eq. (3).

$$T = N^N(x) T^N, \text{N= 1, 2,} \quad (3)$$

Where T^N are nodal temperatures. The Galerkin approach presumes δT, the variation field interpolated by the same functions as $\delta T = N^N \delta T^N$ and δT^N and arbitrarily chosen. First and second order polynomials consists of 1D, 2D and 3D for the N^N. With these interpolations the variation eq. (2) rewritten as,

$$\delta T^N \{ \int_V N^N \rho \dot{E} dV + \int_V \frac{\partial N^N}{\partial x} . k . \frac{\partial T}{\partial x} dV = \int_V N^N r dV + \int_{Aq} N^N q dA \} \quad (4)$$

A 8-node brick in a second-order heat-transfer elements [22] used a numerical Gaussian integration rule because with this for the TVG a smooth solution can be achieved.

The heat-transfer through conduction elements are proposed and are based on the combination of piecewise quadratic-interpolation of T^N via the breadth of the element. The iso-parametric interpolation functions, for the element associated with heat-conduction reference surface, utilised. T^N coupled at a set of points via the breadth at each node of the element (nodes N). For computational numerical integration of the finite-element equations, a 2 × 2 Gauss integration scheme with a 2 × 2 nodal integration scheme used for the internal energy and specific heat term used for the quadrilateral element with 3 × 3 Gauss integration method.

Let $(\emptyset_1, \emptyset_2)$ be individual TVG element directs to the reference surface point of the element related with heat-conduction, and s_3 measures the position through the thickness of the heat conduction object such as edge-seal, glass panes and support pillars so that $-h/2 - z_0 \leq s_3 \leq h/2 - z_0$, where h is the thickness of the element, z_0 is the offset of the reference surface from the mid-surface. The position of any point in the element given by eq. (5).

$$x = x^0(\emptyset_1, \emptyset_2) + s_3 n(\emptyset_1, \emptyset_2) \quad (5)$$

Where x^0 is the locus and n the unit normal of a point in the reference surface. The interpolation of the temperature written as in eq. (6),

$$T = N^N(\emptyset_1, \emptyset_2) M^P(s_3) \dot{T}^{NP} \tag{6}$$

Where, $M^P(s_3)$ is a piecewise parabolic interpolation, $N^N(\emptyset_1, \emptyset_2)$ the interpolator in the reference surface, and $\dot{T}^{NP}$ are nodal temperature values (at node N, point P via the breadth). The thermal-energy balance eq. (2) now rewritten as eq. (7) that accounts heat conduction of each element with the approximate Jacobian matrix for the Newton method.

$$\int_V \rho \delta T \frac{d\dot{E}}{dT_{t+\Delta t}} dT dV + \int_V \frac{\partial \delta T}{\partial x} . k . \frac{\partial dT}{\partial x} dV - \int_A \delta T \frac{\partial q}{dT_{t+\Delta t}} dT \, dA \tag{7}$$

Where dT is the correction to the temperature solution at time $t + \Delta t$. The form of these terms for the elemental heat conduction, e.g. through edge seal and support pillars, is obtained by introducing the interpolator, and neglecting the change in area, with respect to s_3 of surfaces parallel to the reference surface. The piecewise quadratic interpolation via the breadth finite-elements then represented by eq. (8).

$$\left\langle \frac{\partial T}{\partial s_1} \middle| \frac{\partial T}{\partial s_2} \middle| \frac{\partial T}{\partial s_3} \right\rangle = [\gamma^P] \left\langle T^P \middle| \frac{\partial T^P}{\partial s_1} \middle| \frac{\partial T^P}{\partial s_2} \right\rangle \tag{8}$$

Where γ^P one-step operator for stabilising the heat-transfer processes and the elemental heat-transfer through convection modelled with non-symmetric Jacobian matrix, both transient and steady-state capabilities are incorporated. The transient capability introduces a limit on the time increment; the time increment adjusted to satisfy this limit. eq. (9) matched to the work by Yu and Heinrich (1986) [23] and Yu and Heinrich (1987) [24].

$$\int \delta T \left[\rho c \left\{ \frac{\partial T}{\partial t} + v . \frac{\partial T}{\partial x} \right\} - \frac{\partial}{\partial x} \left(k . \frac{\partial T}{\partial x} \right) - q \right] dV + \int_{A_q} \delta T \left[n . k . \frac{\partial T}{\partial x} - q_s \right] dA = 0 \tag{9}$$

Where, $T(x,t)$ the temperature distribution; $\delta T(x,t)$ arbitrary variation field; $\rho(T)$ the fluid density; $c(T)$ the specific-heat of the air molecules which then be reduced for the perfect vacuum; $k(T)$ the conductivity of the air molecules at a particular pressure; q the auxiliary-heat distribution in volume; q_s the surface heat distribution per volume where temperature is not prescribed (A_q); n the outward normal to the surface; x spatial position; and t time. Although low-pressure air in the cavity will have isotropic conductivity, so that $k = kI$ (where $k(T)$ scalar and I unit matrix). The boundary conditions are that T(x) is coupled to A_q and heat flux inflowing the domain across the rest of the surface,$q_s(x)$, is associated by convection and/or radiation conditions and is expressed in eq. (10).

$$q_s = -\mathrm{n}.\mathrm{k}.\frac{\partial T}{\partial x} \tag{10}$$

Where, q_s the heat flux linked to the conduction through the surface only, any convection of energy across the surface not included in q_s. It made negligible variance if the surface is part of a solid body (where q_s defined by heat-transfer into the adjacent body), since then the normal velocity into that body, v.n=0, due to no continuous fluid crossing the surface and here assumed as static conditions in a TVG.

The elemental heat-transfer through radiation is dependent on the surfaces that are comprised of facets with radiation boundary conditions. In this 3D FEM, a facet is a face of a solid element of TVG and each facet presumed to be isothermal having unvarying emissivity. Cavity heat-radiation elements, calculated through Abaqus, produce a series of matrices since they couple the temperature degrees-of-freedom of every node on the cavity surface. Such method of surface radiation is followed

according to Holman (1990) [25] and Howell et al (2010) [26]. Radiation flux density q_j^c into a cavity facet j stated in eq. (11) depends on the grey body radiation theory in which the monochromatic emissivity of the facets is independent of the wavelength of propagation of the radiation and only non-directional reflection applied with the approximation of isothermal and iso-emissive cavity facets.

$$\sum_j \left(\delta_{ij} = (\varepsilon_j - 1)F_{ij}\right)\frac{q_j^c}{\varepsilon_j} = \sigma \sum_j F_{ij}\left(\left(T_j - T^z\right)^4 - (T_i - T^z)^4\right) \quad (11)$$

Where $\varepsilon_i, \varepsilon_j$ are the surface-emissivities of facets i, j ; σ the Stefan-Boltzmann constant; F_{ij} the geometrical view factor matrix; T_i, T_j the temperatures of facets i, j; T^z the value of absolute zero on the temperature scale being used; δ_{ij} is the Kronecker delta. Distinctively, the blackbody radiation, where no reflection takes place, addition of all emissivities equal to one and eq. (11) condensed to eq. (12).

$$q_i^c = \sigma \sum_j F_{ij}\left(\left(T_j - T^z\right)^4 - (T_i - T^z)^4\right) \quad (12)$$

The radiation flux q_i^c is made up of finite element facets occurs when the heat is exchanged that is dependent on view factors, which is a dimensionless factor F_{ij} between two elementary areas, A_i and A_j, satisfies the relation of eq. (13).

$$A_i F_{ij} = \int_{A_i}\int_{A_j} \frac{cos\emptyset_i cos\emptyset_j}{\pi R_{ij}^2}\, dA_i dA_j \quad (13)$$

Where R_{ij} the gap between two areas and $\emptyset_i$, $\emptyset_j$ the angles between R_{ij}. The dimensionless view factor is a geometrical number and for the validation of the accuracy of the calculations eq. (14) used, it is a result of the fact that all rays from facet $\boldsymbol{i}$ collide with other surface $\boldsymbol{j}$ in an enclosed cavity.

$$\sum_j F_{ij} = 1 \quad (14)$$

To reduce the computational time and due to symmetrical conditions, one quarter (150 mm x 150 mm) of the TVG size of 300 mm x 300 mm x 4mm simulated. The model was designed using eight-node linear brick diffusion element, with a total of 174100 elements and 204226 nodes, used to model a quarter of the TVG as shown in Figure 1. The vacuum cavity modelled as a material with thermal conductivity dynamically dependent on the air molecules and its mean free path as most of the thermal conduction occur due to molecules adsorbed on the surfaces and/or left in the cavity of vacuum gap. A 6μm layer, on the inner surface of the glass panes with the emissivity of tin-oxide, coatings modelled for radiation heat-transfer simulations. The stainless steel support pillars modelled as a square, having the side length 1.78r, represented the same heat-transfer as of the cylindrical type used, this approach is used in Fang *et al.* (2006) [27] and Zhao *et al.* (2007) [28]. A graded mesh with a higher number of elements in the pillars employed to achieve adequate representation of the heat-transfer [6, 17]. An example of the finite-element mesh employed as shown in Figure 1. A series of convergence tests performed to ensure that the density of the elements used was sufficient to predict the thermal performance with an accuracy of more than 97%. The material properties and parameters of the simulated triple vacuum glazing listed in Table 1.

Preprints (www.preprints.org) | NOT PEER-REVIEWED | Posted: 23 August 2018 doi:10.20944/preprints201808.0408.v1

Peer-reviewed version available at Appl. Sci. 2018, 8, 1705; doi:10.3390/app8091705

Table 1. Constructional boundary elements of the 10-mm wide edge-sealed TVG.

Type	Boundary	Parametric condition
TVG dimensions	Pane (K Glass) Top	0.3 m x 0.3 m
	Pane (K Glass) Middle	0.3 m x 0.3 m
	Pane (K Glass) Bottom	0.3 m x 0.3 m
	Pane thickness	4 mm
Pilkington K glass pane	Heat conductivity	1 $Wm^{-1}K^{-1}$ [29]
Emittance	low-e coating (each pane)	0.15/SnO_2
Edge seal	Alloy	Cerasolzer CS186
	Width	10 mm
	Heat conductivity	46.49 $Wm^{-1}K^{-1}$*
Support pillar	Alloy	Stainless steel 304
	Diameter	0.3 mm
	Height	0.15 mm
	Pillar separation	24 mm
	Heat conductivity	16.2 $Wm^{-1}K^{-1}$ [16]

[1] Measurement of the thermal conductivity of Cerasolzer CS-186 reported in Memon (2017) [17].

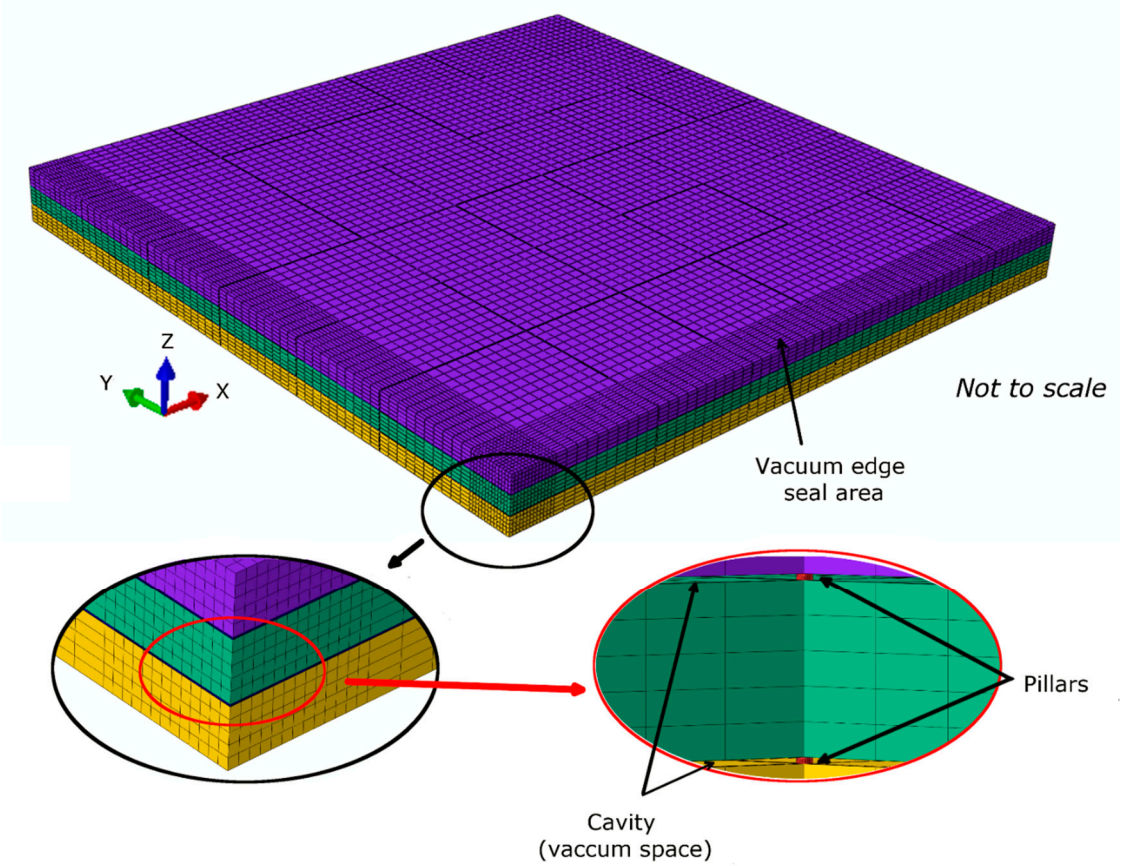

Figure 1. A quarter (size of 150mm x150mm) of 10-mm wide edge sealed triple vacuum glazing showing the developed finite-element mesh.

A thermal contact between glass interfaces with a cavity gap between them specified by incorporating the gap conductance coefficient between two closely adjacent surfaces with small clearance (similar to glass surfaces separated by support pillars). Thermal gap conductance between two surfaces represented by node 1 and 2 with temperatures T_1 and T_2 ($T_1 > T_2$) and clearance d between them is shown in Figure 2.

Peer-reviewed version available at Appl. Sci. 2018, 8, 1705; doi:10.3390/app8091705

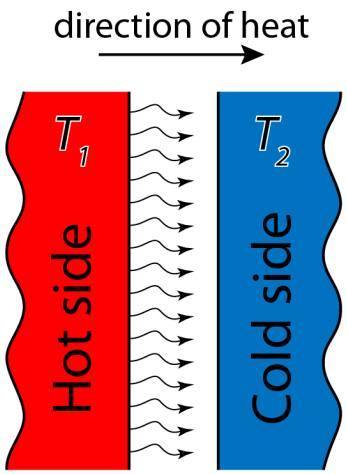

Figure 2. Thermal contact between two interfaces separated by a distance d

The gap heat-transfer defined by the summation of gaseous conductance heat-transfer and radiation heat-transfer between two adjacent surfaces, i.e eq. (15).

$$q_{gap} = q_c + q_r \tag{15}$$

Where q_{gap} the gap heat-transfer, q_c the gas conductance heat-transfer and q_r the radiation heat-transfer. The gas conductance heat-transfer over a fixed gap clearance d given by eq. (16).

$$q_c = k_g(T_2 - T_1) \tag{16}$$

Where k_g the conductance coefficient of the gas, T_1 and T_2 are the temperatures at nodes 1 and 2, respectively. Subroutine GAPCON can help to define the dependency of k_g on different variables including temperature, distance and pressure between the bodies. In this study, it is used to define the k_g as a function of pressure between the glass surfaces [22].

The radiation heat-transfer (q_r) between two nodes in contact is given by eq. (17).

$$q_r = \sigma(T_2 - T_1) \tag{17}$$

Where σ is Stefan-Boltzmann constant, T_1 and T_2 are the temperatures at nodes 1 and 2, respectively. The theoretical model of the thermal gap conductance implemented into Abaqus using the user-defined GAPCON subroutine. When the GAPCON subroutine is called, it provides the pressure and temperatures T_1 and T_2 for the contacting nodes 1 and 2 on adjacent glass surfaces for defining the thermal gap conductance.

The thermal transmittance U value consists of centre-of-pane and total glazing area. The total glazing area contains the edge effects whilst the centre-of-pane do not [30]. The ASTM [31] testing conditions are followed in which the internal and external surface heat-transfer coefficients h were set to 8.3 $Wm^{-2}K^{-1}$ and 30 $Wm^{-2}K^{-1}$, respectively [32] and the internal and external surface air temperatures were set to be at 21.1˚C and -17.8˚C, respectively. The glass surface-to-surface thermal transmittance of the total glazing (U_t) and the centre-of-pane glazing (U_c) defined by eq. (18) and eq. (19).

Peer-reviewed version available at Appl. Sci. 2018, 8, 1705; doi:10.3390/app8091705

$$U_c = \frac{1}{R_{csi} + \frac{q_{ca}}{(T_{cia} + T_{cea})} + R_{cse}} \quad (18)$$

$$U_t = \frac{1}{R_{tsi} + \frac{q_{ta}}{(T_{tia} + T_{tea})} + R_{tse}} \quad (19)$$

Where, R_{csi} and R_{tsi} are the centre-of-pane and total internal surface thermal resistances, respectively, and R_{cse} and R_{tse} are the centre-of-pane and total external surface thermal resistances, respectively. q_{ca} and q_{ta} are the centre-of-pane and total average heat flux by conduction, convection and radiation simulated, using Abaqus, as per the preceding equations, respectively. Similarly, T_{cia} and T_{cea} are the calculated centre-of-pane internal and external average surface-temperatures, respectively. T_{tia} and T_{tea} are the total internal and external average surface-temperatures, respectively.

3. Results and discussion

3.1. Thermal Performance Analysis of 10 mm wide edge-sealed TVG

The U_c and U_t values of 0.28 $Wm^{-2}K^{-1}$ and 0.94 $Wm^{-2}K^{-1}$ was simulated for the triple vacuum glazing at the cavity vacuum pressure of 0.001 Pa and the solar heat gain coefficient (G value) was predicted to be 0.7. A decrease of 15.15% in U_c value and 10.47% in U_t value when compared with the results of Memon et al (2015) [16]. Such decrement in the U_c and U_t values can be attributed to the fact that the secondary edge seal was not used in current model and due to the integration of cavity thermal conductivity assigned to achieve 0.001 Pa (high-vacuum pressure). U_c value of 0.2 $Wm^{-2}K^{-1}$ predicted by Manz et al (2006) [14] for TVG made with 6 mm, 4 mm and 6 mm thick glass panes and four coated surfaces, each of emissivity value of 0.03. Whilst in the present case, all glass panes are 4 mm thick and have three SnO_2 coated surfaces each of emissivity 0.15. By accounting all parameters, the present model is in good agreement with Manz et al (2006) [14] with an error of approximately 4.7%. In comparison to the results of Fang et al [33], U_c value of 0.26 $Wm^{-2}K^{-1}$ and U_t value of 0.65 $Wm^{-2}K^{-1}$, an increase of 7.14% in U_c and 30.85% increase in U_t values, obtained from modelled TVG, was found. Fang et al [33] used 500mm x 500mm size TVG with a 6mm wide edge seal and four coated surfaces each having emissivity of 0.03. One of the potential reasons for such an increase in U_t value obtained from current model linked to edge effects. A 10 mm wide edge seal is used in this study, as compared to 6mm wide, to simulate the design fabricated by the author given elsewhere [16]. Glazing size, due to edge effects, also influence the total thermal transmittance; for TVG size of 500 mm x 500 mm U_t was calculated to be 38% greater than that of a 1 m x 1 m glazed area (Fang *et al* [34]). The emissivity of the surface coatings used in this study is 0.15 as compared to that of 0.03 in literature. A model with same sample size, surface emissivity and seal materials' properties developed to validate the method and results were in good agreement to those presented by Fang *et al* [34] with an error of 6.3%.

The isothermal temperature distribution of the simulated TVG for the cold-side, middle and warm-side surfaces, as shown in Fig 3-5, illustrate significant heat-transfer characteristics necessary in assessing the performance of TVG at high-vacuum pressure. In which the heat flux from the warm-side of the space in a building applied to the indoor glass surface, the thermal radiation between two inner glass surfaces, heat conduction via edge-seal and support pillars, and the heat flux from the outdoor (cold) surface of the glass to the outdoor ambient as per ASTM standard temperatures [35]. The average warm-side (indoor) and cold-side (outdoor) surface temperatures simulated to be 19.22˚C and -9.44˚C of the total surface area, respectively. Whilst, 20.14˚C and -14.13˚C of the centre-of-pane surface area, respectively.

Preprints (www.preprints.org) | NOT PEER-REVIEWED | Posted: 23 August 2018 doi:10.20944/preprints201808.0408.v1

Peer-reviewed version available at Appl. Sci. 2018, 8, 1705; doi:10.3390/app8091705

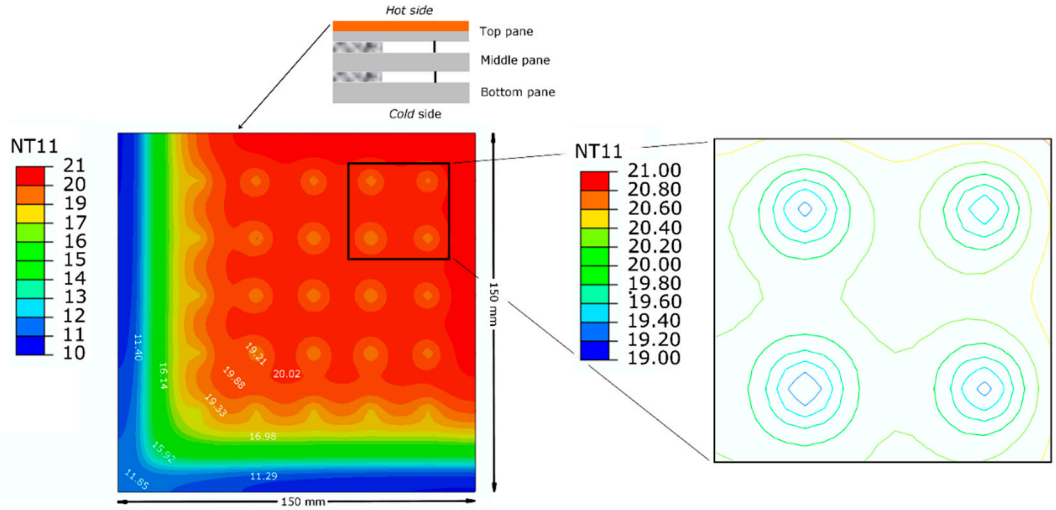

Figure 3. The isothermal temperature distribution on the warm-side glass pane surface of TVG showing the temperature disparities from the 10-mm wide edge-seal area towards the centre-of-pane area due to the use of 10 mm wide edge-seal.

Figure 3 shows the simulated warm-side isothermal temperature distribution of the surface of TVG showing the temperature dissimilarity from the edge area headed to the central area and around the support pillars in the central-glazing area. The temperature difference between the heat conduction through the support pillars and radiative heat flow in the central high-vacuum area predicted to be 1.4°C.

The isothermal temperature distribution for the middle-glass surface facing the warm side, Figure 4a, and cold-side, Figure 4b, of TVG show heat-distribution from the edge area distributed to the central area of the one quarter crossing through the support pillars, in which the heat flow across support pillars larger than that over the vacuum area.

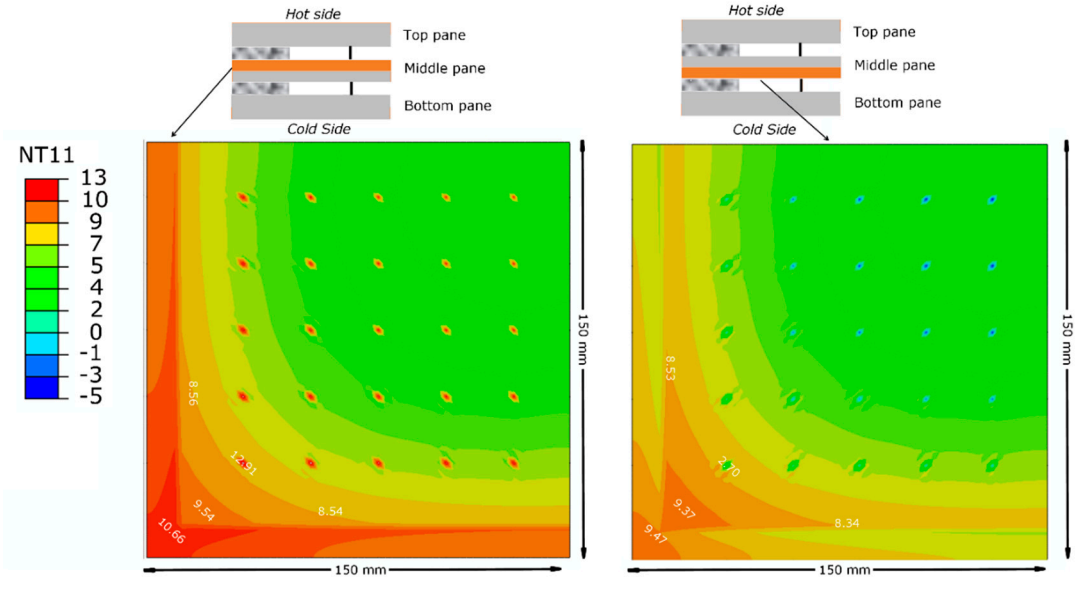

(a) (b)

Figure 4. Isothermal temperature distribution on middle-glass surface facing (a) the warm-side and (b) cold-side of TVG showing the temperature disparities from the 10-mm wide edge-seal area towards the centre-of-pane area.

Peer-reviewed version available at Appl. Sci. 2018, 8, 1705; doi:10.3390/app8091705

The simulated isotherms for the cold-side surface f TVG, in which the heat distribution due to the edge seal and the support pillar array influences the thermal transmittance value, as shown in Figure 5. The variance in temperature was due to the pillar heat-conductance and radiative heat flow over the central vacuum area predicted to be 2.1˚C.

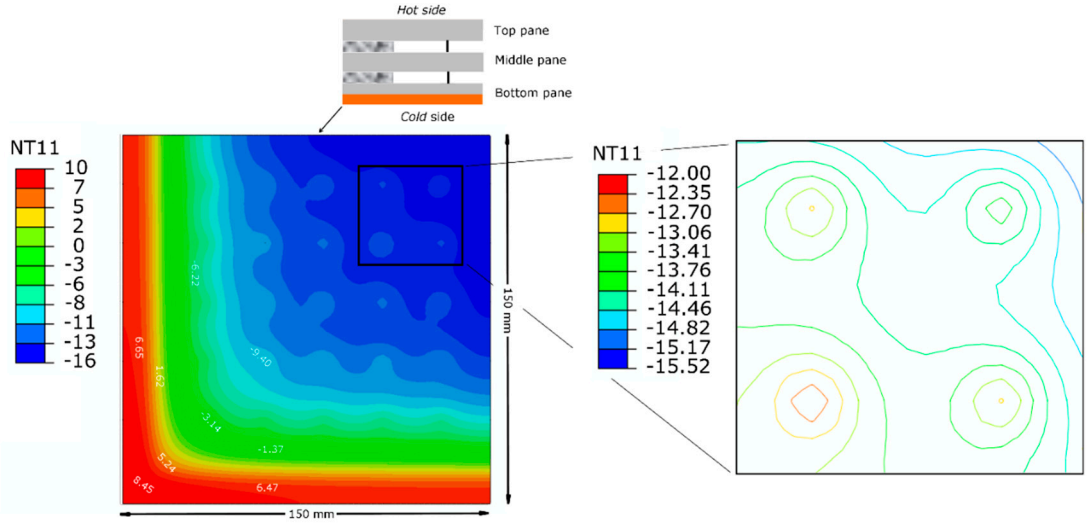

Figure 5. The isothermal temperature distribution on the cold-side glass pane surface of TVG showing the temperature disparities from the 10-mm wide edge-seal area towards the centre-of-pane area.

3.1. Effect of vacuum pressure diminution on the thermal performance of TVG

A vacuum insulation is a cavity, not an empty space between two glass panes as there is no concept of the absolute emptiness in high-vacuum physics but a reduced mass of atmospheric-air. The density of air in a space determines the level of vacuum pressure [36]. This provides thermal insulation, because with a lower density of air the mean free path between air molecules enlarged to above 1000 m, which eventually lowers the heat-transfer path between air molecules in a space. In TVG (current study), the space between glass panes is sealed with hermetic edge seal i.e. Cerasolzer CS-186 and evacuated to high-vacuum pressure 0.001 Pa with the intention of lowering conductive and convective heat-transfer to the trifling value. However, the radiation heat-transfer curtailed using low-emittance SnO_2 coatings. The influence of vacuum pressure decrement due to the vacuum edge seal that usually caused by either degradation due to adsorption of gaseous molecules, mechanical handling and/or inconsistent making of the edge-seal or the edge-seal is not contingent. The FEM results, as shown in Figure 6, predict that when increasing the cavity pressure from 0.001 Pa to 100 kPa the U_c and U_t values increased from 0.28 $Wm^{-2}K^{-1}$ and 0.94 $Wm^{-2}K^{-1}$ to 2.4 $Wm^{-2}K^{-1}$ and 2.58 $Wm^{-2}K^{-1}$, respectively. However, due to ageing process, the TVG may lose the vacuum pressure and it would affect its thermal performance, mainly because of the water vapours evolved from the glass surfaces during the fabrication, which had not desorbed from the glass surfaces and remained in the vacuum space. Thus, the use of non-evaporable getters sealed under specific temperature cycles is necessary. This is because water molecules that outgassed during a high temperature thermal ageing and re-adsorbed onto the glass surfaces at room temperatures can ruin the stability of the internal vacuum pressure unless non-evaporable getter obtain activation.

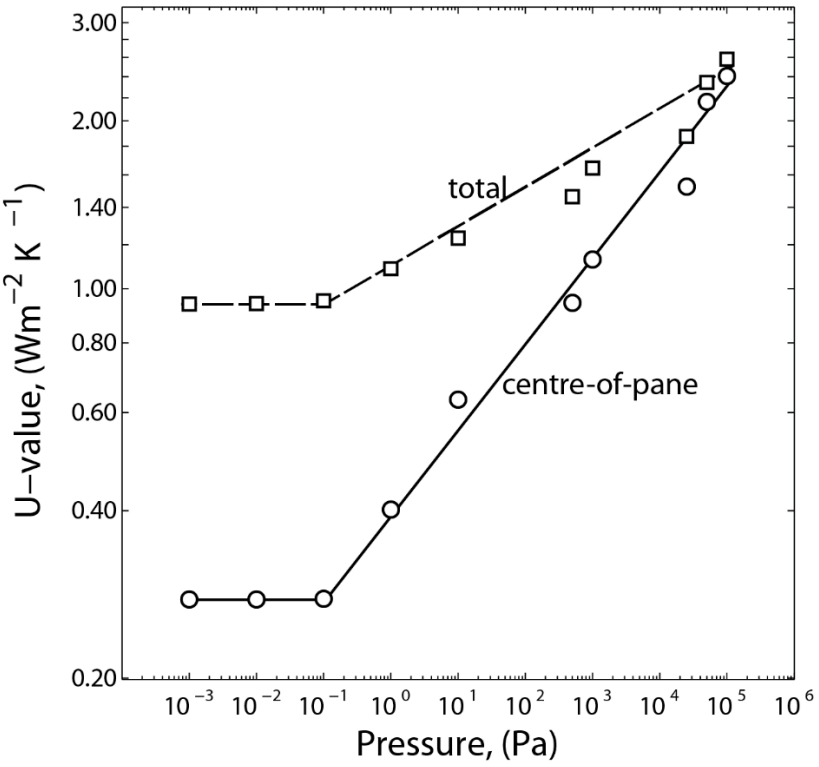

Figure 6. FEM simulated results of the effect of vacuum pressure diminution, between the two cavities each 0.15mm in height, degradation on the U_c and U_t values of TVG.

Figure 7 shows the surface temperature contours for hot and cold side, at the cavity pressure of 0.001 Pa, 1 Pa and 50 kPa, spreading from the vacuum edge seal to the centre-of-pane of one quarter of the TVG along line B and Line A. It shows that the temperature gradients between hot and cold sides increase by decreasing the cavity vacuum pressure from 50 kPa to 0.001 Pa. A reduction in cavity vacuum pressure affects the surface heat-transfer quite significantly. However, the temperature gradients on the cold side are larger than on the warm side due to the direction of the heat flow on the hot side dissipating heat through the edge seal influencing towards the centre-of-pane area. Consequently developing edge effects that spread up to distances of 38 mm and 70 mm from the edge to the centre-of-pane on the hot and cold side surfaces along the Line A (which is nearer to the edge-corners). Nevertheless, at 50 kPa the edge effects to the centre-of-pane are smaller along line A (about 26 mm and 30 mm on hot and cold side, respectively) because of the diminution of the vacuum pressure affecting temperature gradients. Line B is approximately 130 mm away from the horizontal axis of the TVG quarter; it shows the edge effects reduces when moving away from the edge corners. When comparing the surface temperature contours along the line A and line B on the hot and cold side, the temperature gradients on the line B was increased to the line A at cavity vacuum pressure of 0.001 Pa and 1 Pa. By reducing the width of the edge seal, further reduction to the edge effects achievable. A negligible difference in temperature gradients predicted at the cavity vacuum pressure of 50 kPa of the TVG, which effectively increases the heat transmission with less influence of the edge seal.

Preprints (www.preprints.org) | NOT PEER-REVIEWED | Posted: 23 August 2018 doi:10.20944/preprints201808.0408.v1

Peer-reviewed version available at Appl. Sci. 2018, 8, 1705; doi:10.3390/app8091705

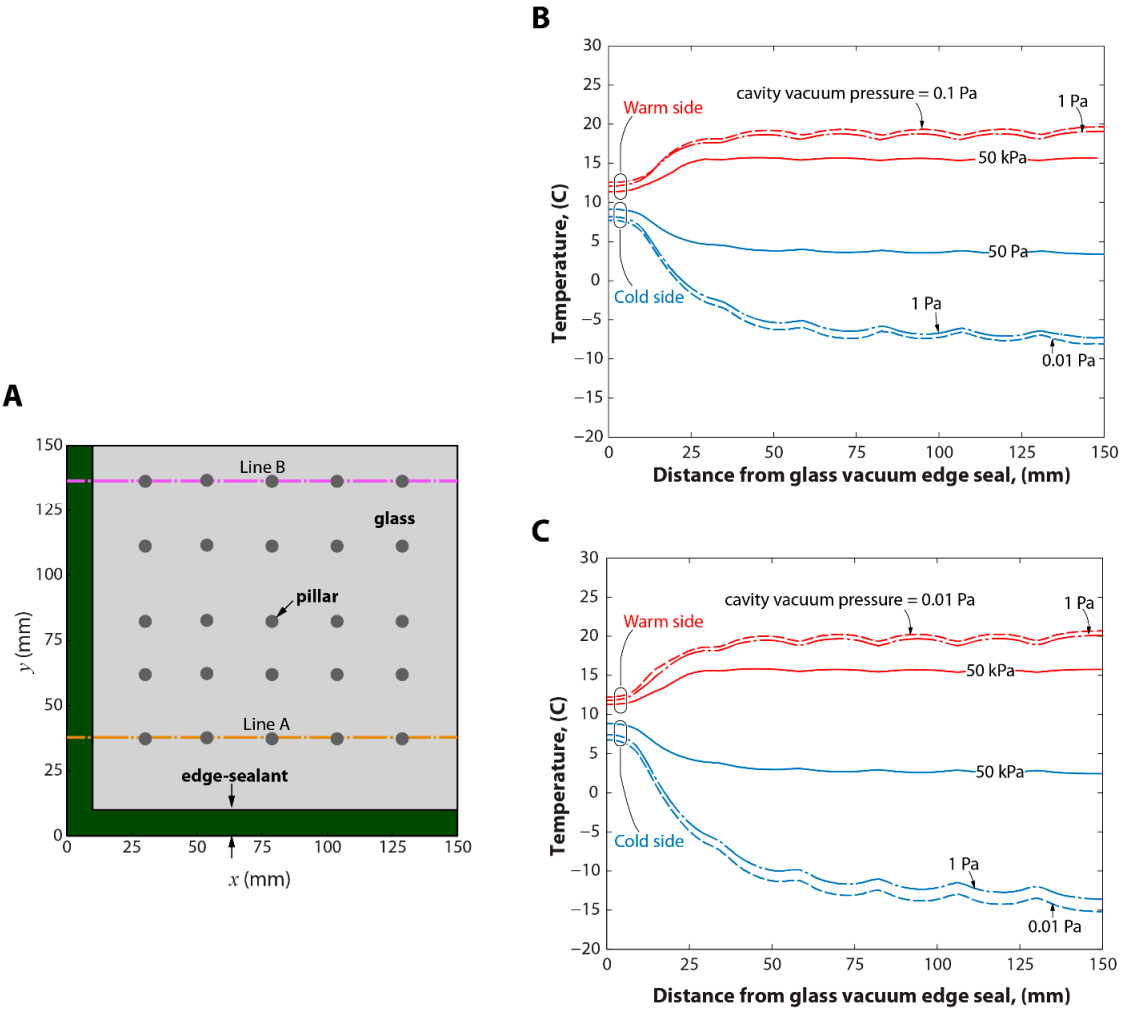

Figure 7. (a) The surface temperature contours for hot and cold side, at the cavity pressure of 0.001 Pa, 1 Pa and 50 kPa, spreading from the vacuum edge seal to the centre-of-pane of one quarter of the TVG (b) along line A and (c) Line B.

5. Conclusions

Long-term durability of the vacuum edge-seal has been the paramount requirement, specifically, in the evolution of TVG for the potential retrofit to existing buildings in achieving them towards NEB. For this, it has long been estimated but never been reported quantitatively the diminution of vacuum pressure influence on the thermal performance of TVG. In this study, a 3D finite element model, with validated mathematical methods, utilised for the assessment of the influence of vacuum pressure diminution on the thermal performance of a 10 mm wide edge sealed triple vacuum glazing. Finite element model validated with mathematical methods and by comparing the results with those in literature. U_c and U_t values calculated from current model were in good agreement with those measured by Manz et al (2006) [14] and Fang et al (2010) [33]. The U_c and U_t values in the FEM model of TVG were predicted to be 0.28 $Wm^{-2}K^{-1}$ and 0.94 $Wm^{-2}K^{-1}$ at the cavity vacuum pressure of 0.001 Pa. The results suggests that when increasing the cavity pressure from 0.01 Pa to 100 kPa the U_c and U_t values increased from 0.28 $Wm^{-2}K^{-1}$ and 0.94 $Wm^{-2}K^{-1}$ to 2.4 $Wm^{-2}K^{-1}$ and 2.58 $Wm^{-2}K^{-1}$, respectively. It indicates that when a decrement of vacuum pressure occurs it will make the thermal performance inadequate and the use of non-evaporable getters resolve the degradation issue. It concluded that the glass surface temperature gradients between hot and cold sides' increases by decreasing the cavity vacuum pressure from 50 kPa to 0.001 Pa. The influence of cavity vacuum pressure decrement affects the surface heat-transfer quite significantly and the edge effects that

spread up to distances of 38 mm and 70 mm from the edge to the centre-of-pane on the hot and cold side surfaces when contoured along the line A that is nearer to the edge-corners. The edge effects reduces when moving away from the specimen edge. By reducing the width of the edge seal, the edge effects could further be minimised. A negligible difference in temperature gradients predicted at the cavity vacuum pressure of 50 kPa of the TVG, which effectively increases the heat transmission with less influence of the edge seal. With 50 kPa, the edge effects to the centre-of-pane are smaller along line A (about 26 mm and 30 mm on hot and cold side, respectively) because of the diminution of the vacuum pressure affecting temperature gradients. It is also important to take the ageing and high temperature exposure issues into account when it comes to the degradation of the vacuum pressure inside the cavity due to ineffective evacuation of cavity, improper pump-out sealing and the remainder residues of air or moisture molecules in the cavity (that boosts the production of CO, CO_2, H_2O and/or H_2 inside the cavity). Such issues could be solved by utilising non-evaporable getters that require activation temperature of more than 400°C and/or pre-activated combo-getters. It is recommended that without getters, the stability of vacuum pressure of 0.001 Pa for over 20 years of life span in the cavity of 10 mm wide edge sealed triple vacuum glazing is difficult to achieve even under controlled environment.

Author Contributions: conceptualization, methodology, mathematical modelling, wrote the paper, S.M; software, validation, formal analysis, review and editing, F. F., S.M., K. K.

Funding: This research received no external funding and The APC was funded by London South Bank University.

Acknowledgment: This work supported by the self-initiated research collaboration between London South Bank University, UK and De Montfort University, UK.

Conflicts of Interest: The authors declare no conflict of interest.

References

1. Hansen, J.; Makiko, S. Regional climate change and national responsibilities, *Environmental Research Letters* **2016**, 11, no. 3 034009, doi:10.1088/1748-9326/11/3/034009.
2. Yaddanapudi, H. S.; Hickerson, N.; Shrikant, S.; Tiwari, A. Fabrication and characterization of transparent wood for next generation smart building applications, *Vacuum*, **2017**, 146, 649-654, https://doi.org/10.1016/j.vacuum.2017.01.016.
3. Memon, S.; Eames, P.C. Solar Energy Gain and Space-Heating Energy Supply Analyses for Solid-Wall Dwelling Retrofitted with the Experimentally Achievable U-value of Novel Triple Vacuum Glazing, *Journal of Daylighting*, **2017**, 4 (1), 15-25, http://dx.doi.org/10.15627/jd.2017.2.
4. Memon, S.; Eames, P.C. Predicting the solar energy and space-heating energy performance for solid-wall detached house retrofitted with the composite edge-sealed triple vacuum glazing, *Energy Procedia*, **2017**, 122, 565-570, https://doi.org/10.1016/j.egypro.2017.07.419.
5. Memon, S. Analysing the potential of retrofitting ultra-low heat loss triple vacuum glazed windows to an existing UK solid wall dwelling, *International Journal of Renewable Energy Development*, **2014**, 3(3), 161-174, https://doi.org/10.14710/ijred.3.3.161-174.
6. Memon, S. Design, fabrication and performance analysis of vacuum glazing units fabricated with low and high temperature hermetic glass edge sealing materials, PhD dissertation, Loughborough University, **2013**, https://dspace.lboro.ac.uk/2134/14562.
7. Fang, Y.; Eames, P.C.; Norton, B.; Hyde, T.J. Experimental validation of a numerical model for heat transfer in vacuum glazing, *Solar Energy*, **2006**, 80, no. 5, 564-577, https://doi.org/10.1016/j.solener.2005.04.002
8. Benson, D. K.; Tracy, C. E. Evacuated window glazings for energy efficient buildings, In Optical Materials Technology for Energy Efficiency and Solar Energy Conversion IV, *International Society for Optics and Photonics*, **1985**, 562 (1985) 250-256, doi: 10.1117/12.966313.
9. Eames, P.C. Vacuum glazing: current performance and future prospects, *Vacuum*, **2008**, 82, no. 7, 717-722, https://doi.org/10.1016/j.vacuum.2007.10.017.
10. Robinson, S.J.; Collins, R.E. Evacuated windows-theory and practice, *In ISES solar world congress*, international solar energy society, Kobe, Japan. **1989**.
11. Collins, R.E.; Tang, J.Z. Design improvements to vacuum glazing, *U.S. Patent*, **1999**, 5,891,536.

12. Griffiths, P.W.; Leo, M.D.; Cartwright, P.; Eames, P.C.; Yianoulis, P.; Leftheriotis, G.; Norton, B. Fabrication of evacuated glazing at low temperature, *Solar Energy*, **1998**, 63, no. 4, 243-249, https://doi.org/10.1016/S0038-092X(98)00019-X.
13. Zhao, J.F.; Eames, P.C.; Hyde, T.J.; Fang, Y.; Wang, J. A modified pump-out technique used for fabrication of low temperature metal sealed vacuum glazing, *Solar Energy*, **2007**, 81, no. 9, 1072-1077, https://doi.org/10.1016/j.solener.2007.03.006.
14. Manz, H.; Brunner, S.; Wullschleger, L. Triple vacuum glazing: Heat transfer and basic mechanical design constraints, *Solar Energy*, **2006**, 80, no. 12, 1632-1642, https://doi.org/10.1016/j.solener.2005.11.003.
15. Memon, S. Investigating energy saving performance interdependencies with retrofit triple vacuum glazing for use in UK dwelling with solid walls, *Sustainable Development on Building and Environment: Proceedings of the 7th International Conference*, **2015**, ISBN-13: 978-0993120701, Reading, UK.
16. Memon, S.; Farukh, F.; Eames, P.C.; Silberschmidt, V.V. A new low-temperature hermetic composite edge seal for the fabrication of triple vacuum glazing, *Vacuum*, **2015**, 120, 73-82, https://doi.org/10.1016/j.vacuum.2015.06.024.
17. Memon, S. Experimental measurement of hermetic edge seal's thermal conductivity for the thermal transmittance prediction of triple vacuum glazing, *Case Studies in Thermal Engineering*, **2017**, 10, 169-178, https://doi.org/10.1016/j.csite.2017.06.002.
18. Turner, G.M.; Collins, R.E. Measurement of heat flow through vacuum glazing at elevated temperature, *International journal of heat and mass transfer*, **1997**, 40, no. 6, 1437-1446, https://doi.org/10.1016/S0017-9310(96)01895-4.
19. Fang, Y.; Hyde, T.; Eames, P.C.; Hewitt, N. Theoretical and experimental analysis of the vacuum pressure in a vacuum glazing after extreme thermal cycling, *Solar Energy*, **2009**, 83, no. 9, 1723-1730, https://doi.org/10.1016/j.solener.2009.03.017.
20. Ng, N.; Collins, R.E.; So, L. Thermal and optical evolution of gas in vacuum glazing. *Materials Science and Engineering: B*, **2005**, 119, no. 3, 258-264, https://doi.org/10.1016/j.mseb.2004.12.079.
21. Green, A.E.; Naghdi, P.M. A general theory of an elastic-plastic continuum. *Archive for rational mechanics and analysis*, **1965**, 18, no. 4, 251-281.
22. Manual, A.U. Abaqus Theory Guide, **2014**.
23. Yu, C.C.; Heinrich, J.C. Petrov-Galerkin methods for the time-dependent convective transport equation, *International journal for numerical methods in engineering*, **1986**, 23, no. 5, 883-901, https://doi.org/10.1002/nme.1620230510.
24. Yu, C.C.; Heinrich, J.C. Petrov—Galerkin method for multidimensional, time-dependent, convective-diffusion equations, *International Journal for numerical methods in engineering*, **1987**, 24, no. 11, 2201-2215, https://doi.org/10.1002/nme.1620241112.
25. Holman, J.P. Heat Transfer, McGraw-Hill, Inc, New York, **1990**.
26. Howell, J.R.; Menguc, M.P.; Siegel, R. Thermal radiation heat transfer. CRC press, **2010**, ISBN: 9781498757744.
27. Fang, Y.; Eames, P.C.; Norton, B.; Hyde, T.J. Experimental validation of a numerical model for heat transfer in vacuum glazing, *Solar Energy*, **2006**, 80, no. 5, 564-577, https://doi.org/10.1016/j.solener.2005.04.002.
28. Zhao, J.F.; Eames, P.C.; Hyde, T.J.; Fang, Y.; Wang, J. A modified pump-out technique used for fabrication of low temperature metal sealed vacuum glazing, *Solar Energy*, **2007**, 81, no. 9, 1072-1077, https://doi.org/10.1016/j.solener.2007.03.006.
29. Memon, S.; Eames, P.C. Heat load and solar gain prediction for solid wall dwellings retrofitted with triple vacuum glazing for selected window to wall area ratios. *In World Renewable Energy Forum, WREF*, **2012**, 6 4636-4643. ASES, Denver, USA.
30. Collins, R.E.; Robinson, S.J. Evacuated glazing, *Solar Energy*, **1991**, 47, no. 1, 27-38.
31. Wang, J.; Eames, P.C.; Zhao, J.F.; Hyde, T.; Fang, Y. Stresses in vacuum glazing fabricated at low temperature, *Solar energy materials and solar cells*, **2007**, 91, no. 4, 290-303, https://doi.org/10.1016/j.solmat.2006.10.007.
32. Fang, Y.; Hyde, T.J.; Hewitt, N.; Eames, P.C.; Norton, B. Comparison of vacuum glazing thermal performance predicted using two and three dimensional models and their experimental validation, In ASME 2008 *Heat Transfer Summer Conference collocated with the Fluids Engineering, Energy Sustainability, and 3rd Energy Nanotechnology Conferences*, **2008**, 133-139. American Society of Mechanical Engineers, doi:10.1115/HT2008-56054.

33. Fang, Y.; Hyde, T.J.; Hewitt, N. Predicted thermal performance of triple vacuum glazing. *Solar Energy*, 2010, 84, no. 12, 2132-2139, https://doi.org/10.1016/j.solener.2010.09.002.
34. Fang, Y.; Hyde, T.J.; Arya, F.; Hewitt, N.; Wang, R.; Dai, Y. Enhancing the thermal performance of triple vacuum glazing with low-emittance coatings, *Energy and Buildings*, **2015**, 97, 186-195, https://doi.org/10.1016/j.enbuild.2015.04.006.
35. Memon, S.; Eames, P.C. Design, development and thermal performance analysis of ultra-low heat loss triple vacuum glazing. *Proceedings of ISES solar world congress*, Abu Dhabi, UAE, 2017, ISBN 978-3-981 465 9-7-6. doi:10.18086/swc.2017.15.04.